

Performance of Fluorescence Correlation Spectroscopy for Measuring Diffusion and Concentration

Jörg Enderlein,^{*,[a]} Ingo Gregor,^[a] Digambara Patra,^[a] Thomas Dertinger,^[a] and U. Benjamin Kaupp^[a]

Fluorescence correlation spectroscopy (FCS) has become an important tool for measuring diffusion, concentration, and molecular interactions of cellular components. The interpretation of FCS data critically depends on the measurement set-up. Here, we present a rigorous theory of FCS based on exact wave-optical calculations. Six of the most important optical and photophysical

factors that influence FCS are studied: fluorescence anisotropy, cover-slide thickness, refractive index of the sample, laser-beam geometry, optical saturation, and pinhole adjustment. Our theoretical framework represents a general attempt to link all relevant parameters of the experimental set-up with the measured correlation function.

Introduction

Fluorescence correlation spectroscopy (FCS) was introduced more than 30 years ago^[1–3] and has experienced a renaissance due to the availability of affordable laser sources with high beam quality and temporal stability, low-noise single-photon detectors, and microscope objectives with nearly perfect imaging quality at high numerical aperture (NA).^[4] FCS has become an invaluable tool for studying the diffusion of molecules,^[5–7] binding and reaction kinetics,^[8–14] single-molecule photophysics,^[15–23] and conformational dynamics of proteins,^[24] for recent reviews see refs. [25–28].

In FCS, time traces of fluorescence intensity, recorded with high temporal resolution, are correlated with replicas of themselves shifted by different time values τ . The result is the so-called autocorrelation function (ACF) shown in Equation (1):

$$g(\tau) = \langle I(t)I(t+\tau) \rangle_t \quad (1)$$

wherein $I(t)$ is the fluorescence intensity at time t and $I(t+\tau)$ is the value at time $t+\tau$; the brackets denote averaging over all values of t . The value of the ACF is a measure of the probability of detecting a photon at time τ if there was a photon detected at time zero. This probability is composed of two different terms; if the two photons detected at time zero and at time τ , respectively, originate from one and the same molecule, they are correlated, producing a time-dependent component of the ACF. Alternatively, if the two photons originate from uncorrelated background or from different non-interacting molecules, the photons are statistically uncorrelated, and thus contribute only a constant offset to the ACF. Thus, the temporal behaviour of the ACF is solely determined by the correlated contributions of photons from individual molecules. In this regard, FCS is a true single-molecule spectroscopy tech-

nique, although the analysis does not explicitly identify single-molecule detection events.

The ACF is shaped by different properties of the fluorescing molecules; on a nanosecond timescale, the ACF shows a steep rise from zero to some maximum within the fluorescence lifetime. This photon antibunching reflects the fact that, after the emission of a photon, a molecule needs to become re-excited and to spend some time in the excited state before it can emit the next photon.^[29] On the nano- to microsecond timescale, the ACF may be influenced by rotational diffusion of the molecule.^[30] On a microsecond timescale, the ACF is dominated by fast processes such as triplet-state dynamics or photo-isomerization.^[15,24] On a millisecond to second timescale, the ACF decays because molecules leave the detection region by diffusion.

The shape of the ACF due to diffusion is determined by the molecule detection function (MDF) and by the diffusion coefficient of the molecules. The amplitude of the ACF is determined by the concentration of molecules. The MDF quantifies the efficiency with which a photon is detected from a fluorescing molecule. The MDF depends on the intensity distribution of the focused laser light and on the efficiency of detecting a photon from its point of origin, but also on the photophysics

[a] Dr. J. Enderlein, Dr. I. Gregor, Dr. D. Patra,* T. Dertinger, Dr. U. B. Kaupp
Institute for Biological Information Processing 1, Forschungszentrum Jülich
52425 Jülich (Germany)
Fax: (+49) 2461-614216
E-mail: j.enderlein@fz-juelich.de

[*] Current address:
Department of Physics, School of Science and Engineering
Okubo 3-4-1, Shinjuku-ku, Tokyo, 169-8555 (Japan)

Supporting information for this article is available on the WWW under <http://www.chemphyschem.org> or from the author.

of the fluorescing molecules and on their rotational diffusion. These factors enter the MDF in a complicated way that does not generally allow the factoring the MDF into a pure excitation and a pure emission part.

In most publications on FCS, the MDF is assumed to have a three-dimensional (3D) Gaussian shape.^[31] This assumption significantly simplifies the calculation of the autocorrelation function, but represents the experimental situation rather imprecisely. Moreover, this assumption introduces arbitrary parameters (the transversal and longitudinal extent of the 3D Gaussian MDF) that are difficult to relate to experimental parameters such as the numerical aperture of the objective or the characteristics of the laser-beam excitation and the confocal detection. Due to the lack of a straightforward relation between the optical parameters of the measurement system and the empirical coefficients describing the shape of the 3D Gaussian, optical misalignment or parameter deviations cannot be taken into account when modeling an FCS experiment.

A first comprehensive study pointing out the fallacy of the 3D Gaussian approximation for FCS was presented in ref. [32], and in ref. [33] we presented a brief nontechnical discussion of the various error sources that can effect the outcome of an FCS measurement. Here, we present a rigorous theoretical treatment of FCS based on exact wave-optical calculations of the complete experimental set-up and systematically study the impact on the ACF of different optical and photophysical factors. In particular, we investigate how these factors affect the apparent values of the diffusion coefficient and concentration. First, we study the influence of polarization (polarization of excitation and detection, and fluorescence anisotropy of sample). Second, we examine three major sources of optical aberration: variation of cover-slide thickness, refractive-index mismatch, and laser-beam astigmatism. Third, we examine the dependence of the MDF on the excitation intensity—a fact that has been well recognized only recently.^[34–36] Finally, we briefly consider the consequences of misalignment of the confocal aperture.

The next section presents a comprehensive theory of FCS, referring to previously published material as much as possible while trying to be self-contained. The reader who is more interested in the final results may skip the next section and move directly to the Numerical Results and Discussion sections.

Theoretical Foundations

Autocorrelation and Diffusion

The standard set-up of a FCS measurement is shown in Figure 1.^[37] Fluorescent molecules are dissolved in an aqueous solution that is placed on a cover slide. A collimated laser beam with a perfect Gaussian TEM₀₀ mode is coupled via a dichroic mirror into an objective with high NA that focuses the laser into a diffraction limited spot in the sample. The dichroic mirror is reflective at the laser's wavelength and transmissive at the wavelengths of the fluorescence emission. Fluorescence light generated in the sample is collected by the same objec-

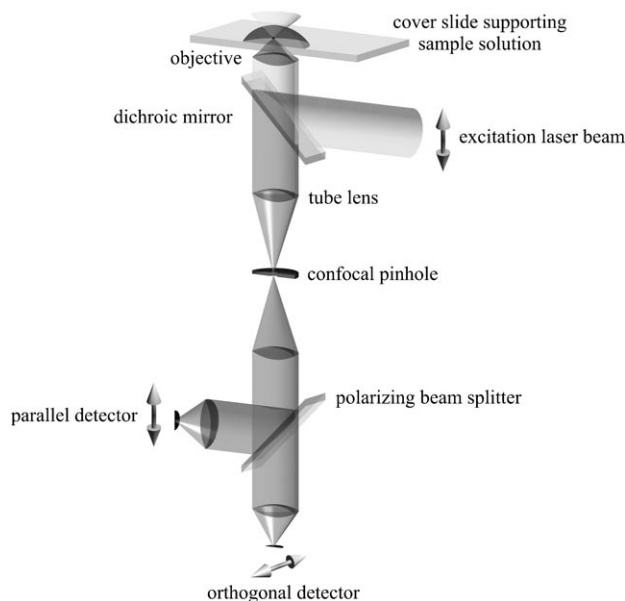


Figure 1. Principal scheme of a confocal epi-fluorescence microscope as used in FCS. Shown is a set-up with a linearly polarized excitation laser. Detection is done with two detection channels after splitting the light with a polarizing beam splitter. The detectors are usually single-photon avalanche diodes or photomultiplier tubes. The vertical position of the objective can be accurately adjusted using a piezoelectric actuator (not shown).

tive (so-called epi-fluorescence set-up), transmitted through the dichroic mirror, and focused onto a circular confocal aperture. Behind the aperture, the fluorescence light is refocused onto a sensitive light detector, usually a single-photon counting photomultiplier tube or a single-photon avalanche diode. The confocal aperture effectively rejects fluorescence light that is generated outside the focal plane. Both the restriction of fluorescence generation (by diffraction-limited focusing) and detection (by confocal detection) generate an effective detection volume of about 0.5 μm in diameter in the focal plane and a few micrometers along the optical axis.

The calculation of the ACF is equivalent to determining the probability of detecting a photon at time $t + \tau$ if there was a photon detected at time t . The fluorescence signal $I(t)$ is composed of the contributions from all fluorescent molecules in the sample and background sources, as shown in Equation (2):

$$I(t) = \sum_j I_j(t) + I_{\text{bg}}(t) \quad (2)$$

where I_j refers to the j th molecule, and the summation considers all N molecules in the sample. I_{bg} denotes the supposedly uncorrelated but fluctuating background signal. Inserting Equation (2) into $g(\tau)$ yields Equations (3a) and (3b):

$$g(\tau) = \sum_j \langle I_j(t) I_j(t + \tau) \rangle + \sum_{j \neq k} \langle I_j \rangle \langle I_k \rangle + 2 \langle I_{\text{bg}} \rangle \sum_j \langle I_j \rangle + \langle I_{\text{bg}} \rangle^2 \quad (3a)$$

$$= N \langle I_1(t) I_1(t + \tau) \rangle + N(N - 1) \langle I_1 \rangle^2 + 2N \langle I_{\text{bg}} \rangle \langle I_1 \rangle + \langle I_{\text{bg}} \rangle^2 \quad (3b)$$

where angular brackets denote averaging over time t . In Equation (3b), I_j refers to the intensity of any of the molecules; all averages are independent of index j (it is assumed that there is only one molecular species within the sample so that each molecule will give, in the limit of infinite averaging time, the same average signal). The physically most significant part of the ACF is the first, time-varying term in Equation (3b). It is proportional to the conditional probability of detecting a fluorescence photon at time $t + \tau$ if there was a photon-detection event from the same molecule at time t . This conditional probability can be calculated as a double integral over a product of four probability functions: 1) the probability that a molecule is found within a volume element $d\mathbf{r}_0$ at position \mathbf{r}_0 , that is, $V^{-1}d\mathbf{r}_0$, where V is the total volume of the solution; 2) the probability density $U(\mathbf{r}_0)$ of detecting a photon from a molecule at position \mathbf{r}_0 , that is, the MDF; 3) the probability density that a molecule diffuses from position \mathbf{r}_0 to position \mathbf{r}_1 within time τ , which is given by the Green's function $G(\mathbf{r}_0 - \mathbf{r}_1, \tau)$ of the diffusion equation in free space shown in Equation (4):

$$G_0(\mathbf{r}_1 - \mathbf{r}_0, \tau) = \frac{1}{(4\pi D\tau)^{3/2}} \exp\left[-\frac{(\mathbf{r}_1 - \mathbf{r}_0)^2}{4D\tau}\right] \quad (4)$$

and 4) the probability density $U(\mathbf{r}_1)$ of detecting a photon from a molecule at position \mathbf{r}_1 . Thus, one arrives at Equation (5):

$$\langle I_1(t)I_1(t + \tau) \rangle = V^{-1} \int d\mathbf{r}_1 \int d\mathbf{r}_0 U(\mathbf{r}_1) G_0(\mathbf{r}_1 - \mathbf{r}_0, \tau) U(\mathbf{r}_0) \quad (5)$$

where both integrations extend over the sample volume V . To find the ACF, we also need the average intensity $\langle I_1 \rangle$, which is given by Equation (6):

$$\langle I_1 \rangle = V^{-1} \int d\mathbf{r} U(\mathbf{r}) \quad (6)$$

Inserting Equations (5) and (6) into $g(\tau)$ yields the final result shown in Equation (7):

$$g(\tau) = c \int d\mathbf{r}_1 U(\mathbf{r}_1) \left[\int d\mathbf{r}_0 G_0(\mathbf{r}_1 - \mathbf{r}_0, \tau) U(\mathbf{r}_0) \right] + \left[c \int d\mathbf{r} U(\mathbf{r}) + I_{\text{bg}} \right]^2 U(\mathbf{r}) = \sum_{m=0}^{\infty} U_m(\rho, z) \cos m\phi \quad (7)$$

where c denotes the concentration of fluorescent molecules (numbers per volume) and we have used the fact that, in the limit of large sample volume, $N/V \rightarrow c$ and $N(N-1)/V^2 \rightarrow c^2$. The ACF, in particular the first term in Equation (7), is correct if the only process correlating the photon detection at different times is the diffusion of the molecules through the detection volume, so that, at any time, the photon-detection probability depends only on the position of the molecules in the sample and is completely described by the MDF. Any additional correlation, connected for example with the photophysical history of a molecule such as fluorescence antibunching, triplet-state dynamics, or any conformational dynamics which change the fluorescence, are completely neglected, but can usually be accounted for by multiplicative exponential terms if such correlations are much faster than the diffusion of the molecule.^[24,38]

An important property of the ACF is that the concentration of the fluorescent species can be derived from Equation (7) via Equation (8):

$$\frac{g(\infty)}{g(0) - g(\infty)} = c \frac{[\int d\mathbf{r} U(\mathbf{r}) + I_{\text{bg}}]^2}{\int d\mathbf{r} U^2(\mathbf{r})} \quad (8)$$

For negligible background I_{bg} one can define the effective detection volume V_{eff} through Equation (9):

$$V_{\text{eff}} = \frac{[\int d\mathbf{r} U(\mathbf{r})]^2}{\int d\mathbf{r} U^2(\mathbf{r})} \quad (9)$$

so that, for negligible background, the left-hand side of Equation (8) equals cV_{eff} , that is, the mean particle number within V_{eff} . Thus, the ACF is often used for estimating concentrations of fluorescing molecules. Below, we will present results concerning the impact of the different experimental conditions on the effective detection volume and thereby the apparent concentration.

Equation (7) shows a simple but numerically important point: to evaluate the double integral in Equation (7), one can first calculate the function $F(\mathbf{r}, \tau)$, which represents the solution to the diffusion equation after time t for initial condition $F(\mathbf{r}, \tau=0) = U(\mathbf{r})$, and subsequently calculate the integral $\int d\mathbf{r} U(\mathbf{r}) F(\mathbf{r}, \tau)$. Although all integrals extend over the sample volume V , the MDF differs significantly from zero only in a very small region: it falls off quickly to zero within a few micrometers from its position of maximum value. Thus, the numerical integration requires only moderate computer memory.

The ACF can be simplified further by taking into account that the MDF is almost symmetric around the optical axis. Using cylindrical coordinates $\mathbf{r} = \{\rho, \phi, z\}$ with the coordinate z oriented along the optical axis, any MDF can be developed in a harmonic series as shown in Equation (10):

where the appearance of only cosine functions in the expansion reflects the bilateral symmetry of the MDF which applies to almost all excitation/detection conditions of practical interest (excitation as well as detection that is well adjusted and centered on the optical axis of the microscope). Inserting the above expansion into the expression found for the ACF and integrating over the angular variables leads to Equations (11) and (12):

$$g(\tau) = \pi c \sum_{m=0}^{\infty} (1 + \delta_{m,0}) \int d\rho \rho \int dz U_m(\rho, z) F_m(\rho, z, \tau) + \left[2\pi c \int d\rho \rho \int dz U_0(\rho, z) + I_{\text{bg}} \right]^2 \quad (11)$$

$$F_m(\rho, z, \tau) = \frac{2\pi i^m \exp(-\rho^2/4D\tau)}{(4\pi D\tau)^{3/2}} \int_0^\infty d\rho_0 \rho_0 \int_{-\infty}^\infty dz_0 U_m(\rho_0, z_0) \quad (12)$$

$$J_m \frac{i\rho\rho_0}{2D\tau} \exp\left[-\frac{\rho_0^2 + (z - z_0)^2}{4D\tau}\right]$$

where J_m denotes Bessel functions of the first kind, and $\delta_{m,0}$ is Kronecker's symbol being unity for $m=0$ and zero otherwise. A modification is necessary if measurements are performed close to an impenetrable interface, so that instead of using the Green's function of the diffusion equation in free space one has to use the Green's function in half space, which is easily realized by replacing the last exponent in Equation (12) with the sum in Equation (13):

$$\exp\left[-\frac{\rho_0^2 + (z - z_0)^2}{4D\tau}\right] + \exp\left[-\frac{\rho_0^2 + (z + z_0 + 2d)^2}{4D\tau}\right] \quad (13)$$

where the d is the z -position of the interface. Although Equations (11) and (12) look more complex than Equation (7), they now involve only double integrals, which are much easier to handle numerically than the original three-dimensional integrals. These equations will be the basis for all subsequent numerical calculations of the ACF. They clearly illustrate the central role played by the MDF as given by the functional coefficients $U_m(\rho, z)$, the knowledge of which completely determines the ACF. Therefore, the next sections will deal with the determination of the MDF.

Molecule Detection Function

In the simplest case, the MDF is given by the product of the excitation light intensity distribution in the sample times the light collection efficiency (CEF) which is defined by the detection optics. As such, the MDF is equivalent to the point-spread function (PSF) of confocal microscopy.^[39,40] However, this equivalence applies only if the fluorescing molecules exhibit sufficiently fast rotational diffusion leading to decoupling between their orientation during light absorption and fluorescence emission. As will be shown below, for slowly rotating molecules the situation becomes more complicated, and the MDF cannot be described by a direct product of excitation light-intensity distribution and the CEF. The situation becomes even more complicated if one considers molecule detection close to a medium with significantly different refractive index than that of the sample solution (e.g. performing FCS near a dielectric or a metallic mirror), leading to a change in the angular distribution of emission.

In the following, we derive a general expression for the MDF that will be the cornerstone for the subsequent calculation and analysis of the ACF. We make the assumption that the fluorescing molecules are electric-dipole absorbers and emitters. However, a generalization is possible for more complex situations such as electronically or photophysically coupled multichromophoric molecules or fluorescent nanocrystals with exotic absorption and/or emission properties.^[41] The derivation of the MDF will proceed in several steps. First, we will describe

the excitation intensity distribution of the focused laser beam in the sample, taking into account possible refractive-index mismatch of the sample solution, inaccurate cover-slide thickness, and small astigmatism of the exciting laser beam. Second, we use the excitation intensity distribution to determine the excitation probability of a molecule within the focal region, taking into account its orientation and photophysics, including possible optical saturation caused by ground state depletion. Third, we deal with the efficiency to detect a fluorescence photon by the confocal detection set-up, taking into account rotational diffusion of the molecules as well as non-collinearity between absorption and emission dipole, interface effects influencing the emission properties of the molecule, refractive index mismatch, and deviations of cover slide thickness. Finally, in a last synthesizing step, all the pieces are put together to obtain the complete MDF.

Excitation Intensity Distribution

The theoretical foundations for calculating the focusing of a laser beam through high-aperture optics were laid by Richards and Wolf.^[42,43] The core idea is to expand the electric field in sample space into a superposition of plane waves and to find the relation between polarization and amplitude of the plane waves and that of the incoming laser beam. This plane-wave representation is ideally suited for taking into account the influence of planar layers between the objective's front lens and the fluorescent molecule, that is, the cover-slide glass or the sample solution. Additionally, we will consider the effect of astigmatism of the exciting laser beam, that is, if the beam has different focal positions in different planes along the axis of propagation.^[44,45] Such astigmatism is easily introduced when using optical fibers for laser-mode cleaning, or when using (dichroic) mirrors with not perfectly flat surfaces. Although astigmatism is often too small to be noticed in the collimated beam before coupling it into the high-NA objective, it can have a significant impact on the MDF after diffraction-limited focusing.

In the paraxial approximation, the electric field amplitude of a linearly polarized astigmatic laser beam is given by Equation (14):

$$\mathbf{E}_0 \sim \frac{\hat{\mathbf{x}}}{w_1 w_2 \sqrt{(1 + \zeta_1^2)(1 + \zeta_2^2)}} \exp\left[-\frac{x^2(1 - i\zeta_1)}{w_1^2(1 + \zeta_1^2)} - \frac{y^2(1 - i\zeta_2)}{w_2^2(1 + \zeta_2^2)}\right] \quad (14)$$

where we have used Cartesian coordinates $\{x, y, z\}$ with z along the axis of propagation, x and y lying within the two principal planes of the beam, and $z=0$ is the position of the back aperture of the objective. The electric field polarization is assumed to be along the x direction. The coordinates $\zeta_{1,2}$ are related to the z -coordinate via $\zeta_{1,2} = \lambda(z - z_{1,2})/\pi w_{1,2}^2$, where $w_{1,2}$ and $z_{1,2}$ are the beam waist diameters and positions in the two principal planes, respectively. In addition, λ is the laser wavelength in air, which has a refractive index close to one. An astigmatic beam is characterized by unequal focus positions z_1 and z_2 , and unequal values of w_1 and w_2 correspond to an elliptic

beam profile. The electric field distribution that is obtained after focusing a beam characterized by Equation (14) was derived in detail in ref. [45] and is described by Equation (15):

$$\mathbf{E}_{\text{ex}}(\rho, \phi, z) = \begin{pmatrix} H_0(\rho, z) + \sum_{q=1}^{\infty} H_{2q}^{(c)}(\rho, z) \cos 2q\phi \\ \sum_{q=1}^{\infty} H_{2q}^{(s)}(\rho, z) \sin 2q\phi \\ \sum_{q=1}^{\infty} H_{2q-1}^{(c)}(\rho, z) \cos(2q-1)\phi \end{pmatrix} \quad (15)$$

where the (ρ, z) -dependent H coefficients involving integrals over Bessel functions. Equation (15) for the electric-field distribution takes into account several experimental peculiarities of an FCS measurement such as variations of cover-slide thickness, refractive-index mismatch between immersion medium and sample solution, or laser-beam astigmatism (for more details, see ref. [45]). Equation (15) is easily generalized for other than x -polarized excitation. A y -polarized beam will generate a field distribution that can be obtained from Equation (15) by replacing $E_{\text{ex},x}$ with $-E_{\text{ex},y}$, $E_{\text{ex},y}$ with $E_{\text{ex},x}$, and ϕ with $\phi - \pi/2$. Any more complex excitation polarization such as circular polarization can be represented as a linear superposition of x - and y -polarized beams.

Fluorescence Excitation Probability and Optical Saturation

For an ideal dipole absorber, the light absorption is proportional to the square of the scalar product between the electric-field amplitude vector \mathbf{E}_{ex} and the normalized dipole vector $\hat{\mathbf{p}}$, that is, $|\hat{\mathbf{p}} \cdot \mathbf{E}_{\text{ex}}|^2$. However, for calculating the ACF, one needs the *average* excitation probability of a molecule at a given position, and this probability depends also on the *optical saturation*. Optical saturation occurs when the excitation intensity becomes so large that the molecule spends more and more time in a non-excitable state, so that increasing the excitation intensity does not lead to a proportional increase in emitted fluorescence intensity, see, for example, ref. [46]. The most common sources of optical saturation are: 1) excited-state saturation, that is, the molecule is still in the excited state when the next photon arrives; 2) triplet-state saturation, that is, the molecule undergoes intersystem crossing from the excited to the triplet state so that it can no longer become excited until it returns back to the ground state; 3) other photoinduced transitions into a nonfluorescing state, such as the photoinduced *cis-trans* isomerization in cyanine dyes, or the optically induced dark states in quantum dots. Although the exact relation between fluorescence emission intensity and excitation intensity can be very complex^[46] and even dependent on the excitation mode (pulsed or continuous wave),^[36] a good approximation of the induced fluorescence intensity is given by the empirical relation in Equation (16):

$$\frac{|\mathbf{E}_{\text{ex}} \cdot \hat{\mathbf{p}}|^2}{1 + I_{\text{ex}}/I_{\text{sat}}} \quad (16)$$

where I_{sat} is the so-called saturation intensity, and I_{ex} is the excitation intensity, which is proportional to $|\mathbf{E}_{\text{ex}}|^2$. It is important to understand that the last relation is an average fluorescence intensity which is established after the photophysical state occupancies of the molecule (occupancies of singlet ground state, singlet excited state, and triplet state) have established a stationary equilibrium with the excitation. Directly upon detection of a fluorescence photon from a molecule this is not the case; at the photon-detection time, the molecule is back to its ground state, and it needs time before the state-occupation probabilities again reach stationary equilibrium. On the nanosecond timescale, this can be measured as photon antibunching, reflecting the equilibration between the ground and excited states; and on the microsecond timescale, a fast exponential decay of the ACF is the result of equilibration between singlet and triplet states (or another non-fluorescing state). Only after these fast relaxation processes is Equation (16) a valid description of the probability to see the next fluorescence photon and is thus suitable for the calculation of the ACF on correlation times longer than the fast relaxation towards the stationary equilibrium. As already mentioned, the fast relaxation can be taken into account by incorporating exponentially decaying terms into the ACF, but it does not affect the long-time diffusion-mediated behavior of the ACF and will not be the topic here.

Rotational Diffusion and Relation between Emission and Absorption Dipole Orientation

Fluorescence excitation is not only dependent on the total excitation intensity, but also on the orientation between absorption dipole and the local electric-field polarization. To elucidate the latter effect, it is useful to split the electric field vector into orientation and amplitude, $\mathbf{E}_{\text{ex}} \equiv \hat{\gamma} E_{\text{ex}}$, where $\hat{\gamma}$ is a unit vector, and E the modulus of the electric field vector, $E_{\text{ex}} = |\mathbf{E}_{\text{ex}}|$. If the electric field is not linearly but elliptically polarized, $\hat{\gamma}$ will be a complex-valued unit vector, where the real and imaginary parts of $\hat{\gamma}$ are the half axes of the ellipse along which the field vector rotates. The complicated structure and distribution of $\hat{\gamma}$ in the diffraction limited focus is shown in Figure 2, assuming the same optical parameters as used in the model results section below. The probability to excite a molecule with absorption-dipole orientation $\hat{\mathbf{p}}$ is proportional to the square of the modulus of the scalar product $|\hat{\gamma} \cdot \hat{\mathbf{p}}|$ (remember that $\hat{\gamma}$ is a complex-valued vector). However, for the description of fluorescence emission we need the orientation of the *emission* dipole. Two peculiarities have to be taken into account: 1) there can be a non-zero angle χ between the emission and absorption dipoles; 2) the molecule randomly reorients between photon absorption and emission. A non-zero angle between absorption and emission dipole leads to an initial angular distribution probability of emission-dipole orientations different from the simple $|\hat{\gamma} \cdot \hat{\mathbf{p}}|^2$ -distribution for the absorption dipole, namely to that shown in Equation (17):

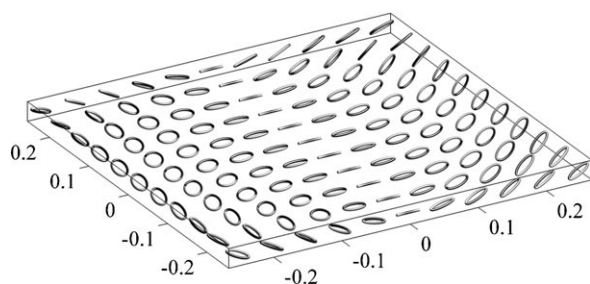


Figure 2. Spatial distribution of the complex polarization structure of a focused laser beam within the focal plane of the objective (values are given in micrometers). The incident laser beam is polarized along the x coordinate. An ellipse corresponds to an elliptically polarized electromagnetic field, the electric field vector rotating along the circumference of the ellipse. Only along the axis $x=0$ does the electric field remain linearly polarized.

$$P_0(\hat{\mathbf{n}}, \hat{\boldsymbol{\gamma}}) = \frac{3}{4\pi} |\hat{\boldsymbol{\gamma}} \cdot \hat{\mathbf{n}}|^2 \left(\cos^2 \chi - \frac{1}{2} \sin^2 \chi \right) + \frac{3}{8\pi} \sin^2 \chi \quad (17)$$

where $\hat{\mathbf{n}}$ is a unit vector along the emission dipole.^[47] The subsequent random reorientation of the molecule can be described by a diffusion equation in angular space (rotational diffusion), leading to a time-dependent distribution $P(\hat{\mathbf{n}}, \hat{\boldsymbol{\gamma}}, t)$. For the sake of simplicity, we will consider here only molecules that behave as isotropic rotators (the rotational diffusion coefficient is independent on rotation axis), which is an excellent approximation for most cases of interest. The incorporation of anisotropic rotators is technically possible but will lead to dramatically more complex relations. For an isotropic rotator, solving the rotational diffusion equation with the initial angular distribution P_0 leads to the time-dependent distribution of emission dipole orientations in Equation (18):^[48]

$$P(\hat{\mathbf{n}}, \hat{\boldsymbol{\gamma}}, t) = \frac{3}{4\pi} \left[\frac{1}{3} + \left(\cos^2 \chi - \frac{1}{2} \sin^2 \chi \right) \left(|\hat{\boldsymbol{\gamma}} \cdot \hat{\mathbf{n}}|^2 - \frac{1}{3} \right) \exp(-6D_{\text{rot}}t) \right] \quad (18)$$

where D_{rot} is the rotational diffusion coefficient. What is needed for the calculation of the ACF is the *temporal average* of this distribution taking into account that the probability of fluorescence photon emission is rapidly decaying on a nanosecond timescale. This leads to the averaged distribution of emission dipole orientations in Equation (19):

$$\bar{P}(\hat{\mathbf{n}}, \hat{\boldsymbol{\gamma}}) = \frac{3}{4\pi} \left[\frac{1}{3} + C_\chi \left(|\hat{\boldsymbol{\gamma}} \cdot \hat{\mathbf{n}}|^2 - \frac{1}{3} \right) \right] \quad (19)$$

where we introduce the abbreviation in Equation (20):

$$C_\chi = \left(\cos^2 \chi - \frac{1}{2} \sin^2 \chi \right) \langle \exp(-6D_{\text{rot}}t) \rangle \quad (20)$$

The angular brackets denote integration over time t with the fluorescence decay curve as a weight function. For a mono-exponential fluorescence decay of $\exp(-t/\tau)$ with fluorescence lifetime τ , one finds $\langle \exp(-6D_{\text{rot}}t) \rangle = (1 + 6D_{\text{rot}}\tau)^{-1}$. The derived distribution $\bar{P}(\hat{\mathbf{n}}, \hat{\boldsymbol{\gamma}})$ is the average distribution of

emission dipole orientations of emitting molecules in dependence on the local excitation-field polarization $\hat{\boldsymbol{\gamma}}$, and is thus also a function of position in space.

Fluorescence Detection Efficiency

The last piece necessary for constructing the MDF is the efficiency with which a fluorescence photon is detected from a molecule at position \mathbf{r} and with emission-dipole orientation $\hat{\mathbf{n}}$. The basic assumption here is that the detection efficiency is proportional to the fluorescence light that passes through the confocal aperture. Thus, one has to calculate the energy flux through the open area of the confocal aperture. This is done in two steps. Firstly, one calculates the angular distribution of radiation generated by the fluorescing molecule directly in front of the light-collecting objective lens, and secondly, one calculates how this angular distribution of radiation is transformed, by the light-collecting optics, into an energy flux through the aperture. The first step involves representing the molecular emission as a sum of plane waves and then tracing each plane wave through the different intervening dielectric layers (i.e. solution and cover slide) through to the objective's front lens. The second step is calculating the energy flux S through the aperture by integrating the axial component of the Poynting vector over the aperture area A using Equation (21):

$$S = \frac{c}{8\pi} \int_A d\mathbf{A} \cdot \text{Re}(\mathbf{E}_{\text{em}} \times \mathbf{B}_{\text{em}}^*) \quad (21)$$

where c is the vacuum speed of light. Calculation of the electric and magnetic fields across the aperture is done similarly to the calculation of the excitation intensity distribution in sample space.^[49–52] Following ref. [52] it can be shown that the electric and magnetic fields in aperture space are given by Equations (22) and (23):

$$\begin{aligned} \mathbf{E}_{\text{em}} = & \{ [F_0(\tilde{\rho}, \tilde{z}) \cos \alpha - F_2(\tilde{\rho}, \tilde{z}) \cos(2\tilde{\phi} - \alpha)] \sin \beta \\ & + F_1(\tilde{\rho}, \tilde{z}) \cos \beta \cos \tilde{\phi} \} \hat{\mathbf{x}} + \{ [F_0(\tilde{\rho}, \tilde{z}) \sin \alpha - F_2(\tilde{\rho}, \tilde{z}) \sin(2\tilde{\phi} - \alpha)] \\ & \sin \beta + F_1(\tilde{\rho}, \tilde{z}) \cos \beta \sin \tilde{\phi} \} \hat{\mathbf{y}} \end{aligned} \quad (22)$$

$$\begin{aligned} \mathbf{B}_{\text{em}} = & \{ [-G_0(\tilde{\rho}, \tilde{z}) \sin \alpha + G_2(\tilde{\rho}, \tilde{z}) \sin(2\tilde{\phi} - \alpha)] \sin \beta \\ & - G_1(\tilde{\rho}, \tilde{z}) \cos \beta \sin \tilde{\phi} \} \hat{\mathbf{x}} + \{ [G_0(\tilde{\rho}, \tilde{z}) \cos \alpha - G_2(\tilde{\rho}, \tilde{z}) \cos(2\tilde{\phi} - \alpha)] \\ & \sin \beta + G_1(\tilde{\rho}, \tilde{z}) \cos \beta \cos \tilde{\phi} \} \hat{\mathbf{y}} \end{aligned} \quad (23)$$

where F_j and G_j are functions involving integrals over Bessel functions, β is the emission-dipole inclination towards the optical axis and α is the angle between its projection into a plane perpendicular to the optical axis and the x axis. The coordinates $\tilde{\rho}$ and $\tilde{\phi}$ refer to a cylindrical coordinate system where $(\tilde{\rho}, \tilde{\phi})$ is the transversal position of the molecule's image in the plane of the confocal aperture (see also Figure 3), and \tilde{z} is the

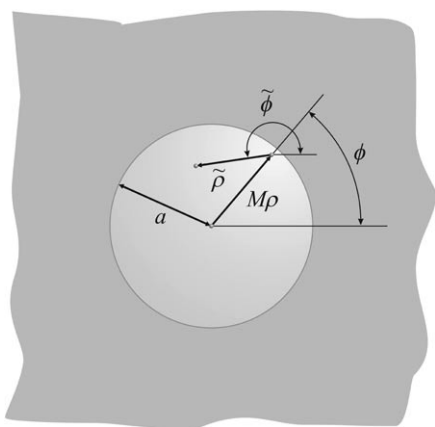


Figure 3. Geometry of the energy flux from one fluorescing molecule through the confocal aperture. The F_i, G_j in Equations (22) and (23) define the energy-flux distribution with respect to a coordinate system centered at the molecule's image position in the aperture plane. That position is a distance $M\rho$ away from the optical axis, where ρ is the radial coordinate of the molecule's position in the sample solution, and M is the magnification of imaging. In this coordinate system, integration over the aperture's area is done by letting $\tilde{\rho}$ run from $(0, M\rho - a)$ up to $M\rho + a$. For every value of $\tilde{\rho}$, the integration limits for $\tilde{\phi}$ are defined by the aperture's edge and explicitly given in Supporting Information.

aperture position along the optical axis within a coordinate system in which $\tilde{z}=0$ defines the image plane. The chosen $(\tilde{\rho}, \tilde{\phi})$ -coordinates are especially useful for performing the two-dimensional integration of the energy flux over the aperture area (see Supporting Information). As a final complication, one has to take into account that the calculated energy flux through the aperture has to be normalized by the total energy flux S_{tot} generated by the molecule into all directions. Only this ratio gives the correct probability that an emitted photon is transmitted through the aperture. Usually, if the molecule is far away from interfaces, S_{tot} does not depend on the molecule's position. However, when performing measurements close to dielectric or metallic surfaces S_{tot} starts to depend on the distance from this interface and the normalization becomes important.^[52] For the sake of completeness let us mention that the above expressions assume nonpolarized detection but can easily be adapted to the presence of a polarizer within the detection channel. For x -polarized detection, for example, one retains in the expression for the electric field \mathbf{E}_{em} only the x component and in the magnetic field \mathbf{B}_{em} only the y component.

Synthesis of the MDF

Finally, the desired MDF is the weighted average of the fluorescence excitation probability times the fluorescence detection probability over all possible emission-dipole orientations, where the weight function is given by the conditional probability distribution $\tilde{P}(\hat{\mathbf{n}}, \hat{\mathbf{y}})$, as shown in Equation (24):

$$U(\mathbf{r}) \propto \frac{E_{\text{ex}}^2(\mathbf{r})}{1 + E_{\text{ex}}^2(\mathbf{r})/I_{\text{sat}}} \int d\hat{\mathbf{n}} \tilde{P}(\hat{\mathbf{n}}, \hat{\mathbf{y}}) \frac{S(\mathbf{r}, \hat{\mathbf{n}})}{S_{\text{tot}}(z, \hat{\mathbf{n}})} \quad (24)$$

The MDF depends on the position of the molecule in sample space, and indirectly on the excitation and emission conditions. As pointed out earlier, it is most convenient to have a representation of the MDF as a Fourier series over the angular variable ϕ . The electric field amplitude distribution of the exciting light can be represented as such a series expansion, see Equation (15). Also, the function $S(\mathbf{r}, \hat{\mathbf{n}})$ is represented by a finite Fourier series (see Supporting Information). To arrive at a Fourier-series expansion for $U(\mathbf{r})$, one expands the factor $(1 + I_{\text{ex}}/I_{\text{sat}})^{-1}$ into a series bringing the ϕ -dependent part into the numerators of the expansion coefficients, and then recursively applies a product formula for Fourier series (see Supporting Information). It is noteworthy that the resulting MDF cannot, in general, be factorized into a simple product of a purely excitation intensity distribution part and a purely fluorescence detection part. This is due to the correlation between excitation- and emission-dipole orientations coupled by rotational diffusion. Only in the limit of infinitely fast rotational diffusion (zero fluorescence anisotropy) can the MDF be factorized. However, for slowly rotating fluorophores or fluorescence labels corotating with a larger tagged molecule, this will not be the case. Another important aspect is that the MDF explicitly takes into account optical saturation, which makes it dependent on excitation intensity. This also makes it different from the standard PSF, which becomes identical to the MDF considered here only in the limit of infinitely low excitation intensity and infinitely fast rotational diffusion.

Numerical Results

To numerically evaluate the ACF via Equations (11) and (12), the MDF coefficients $U_m(\rho, z)$ are discretized on a square (ρ, z) -grid with a grid spacing of $\lambda/30$. The grid extension is chosen large enough that the MDF has fallen below 10^{-3} of its maximum value everywhere. Further refinement or extension of the grid size did not change the resulting ACF. All integrations in Equations (11) and (12) were carried out using finite-element summation. The optical parameters used in the subsequent calculations were chosen to be similar to those of the Confocor 2 system by Carl Zeiss. The Confocor 2 uses an infinity corrected water-immersion objective with 1.2 NA. Image magnification of the sample fluorescence on the 70- μm diameter confocal aperture is $40\times$ employing a tube lens of 164.5-mm focal length. The sample solution is assumed to have the refractive index of water (1.333); the refractive index of the cover-slide glass is assumed to be 1.52. Excitation is done with an Ar-ion laser at 514.5 nm; the laser beam has a Gaussian profile of 5 mm $1/e^2$ -radius, thus matching the objective's back entry of ≈ 4.9 -mm radius and yielding a nearly diffraction-limited focus of about 200-nm radius ($1/e^2$ max. intensity). The laser focus position is set at 200 μm above the cover-slide surface, which is certainly a rather large value but is exactly the design focus position of the Confocor system. Fluorescence emission is assumed to peak around 570 nm. The model diffusion coefficient was set to $5 \times 10^{-5} \text{ cm}^2 \text{ s}^{-1}$. All ratios between apparent and actual diffusion coefficient below were determined by comparing the calculated ACFs with the ideal ACF under ideal optical

conditions (see also ref. [33]). The ratios between the apparent and actual concentration below were determined as the ratios between the ideal and calculated detection volume.

We start by investigating the shape of the ideal MDF if no aberrations are present. To visualize the MDF shape, we will always plot the $1/e^2$ iso-surface, that is, the surface where the MDF has fallen off to $\approx 13\%$ of its maximum value. All calculations assume a linearly polarized excitation laser. Three cases of detection have to be considered: detection through an analyzer parallel to the laser polarization, detection through an analyzer perpendicular to the laser polarization, and unpolarized detection. The three resulting MDFs for the extreme case of a completely anisotropic sample (vanishing rotational diffusion) are visualized in Figure 4. It should be noted that the images do not contain information about the absolute intensity of the detected fluorescence signal, only about the shape of the MDF. For a totally anisotropic sample, fluorescence intensity in the parallel detection channel will be more than twice as large as that in the perpendicular detection channel. However, fluorescence intensity does not affect the MDF and thus has no impact on the ACF. As illustrated by Figure 4, the MDFs for the different detection schemes are very similar, and the resulting ACFs are nearly identical, even in the limit of nonrotating molecules. In a similar arrangement, the difference between the ACFs for unpolarized and polarized excitation is rather marginal. Thus, the influence of the excitation polarization and polarized detection on the diffusion-related part of the ACF can be neglected, and in the following we will consider only polarized excitation with unpolarized detection. It should be noted that the situation dramatically changes when the timescale of the ACF comes close to the average rotation time of the molecules: on that timescale, the behavior of the ACF is influenced by the rotation of the molecules with strong dependence on the polarization properties of excitation and detection. This usually happens on timescales of picoseconds to hundred nanoseconds and can be included into an ACF model in a similar way as, for example, the fast triplet-state dynamics discussed above^[15] and will not be a topic herein.

The next effect studied is the impact of cover-slide thickness on the MDF and thus ACF. Water-immersion objectives are optically corrected for imaging through cover slides of a definite thickness. Advanced objectives offer the possibility to adjust them to a specific thickness value with an adjustment ring. A deviation of the cover-slide thickness from its design value introduces aberration into the optical system, leading to deteriorated laser focusing and fluorescence detection. Although cover slides are sold with a specified thickness value, their actual thickness can differ from that specified by a few percent. We have studied absolute thickness deviations between 0 and 10 μm . The sign of the thickness deviation, that is, whether the cover slide is too thin or too thick, is unimportant: an opposite sign leads to a vertically reflected MDF and an identical ACF. Also, the absolute value of the cover-slide thickness is un-

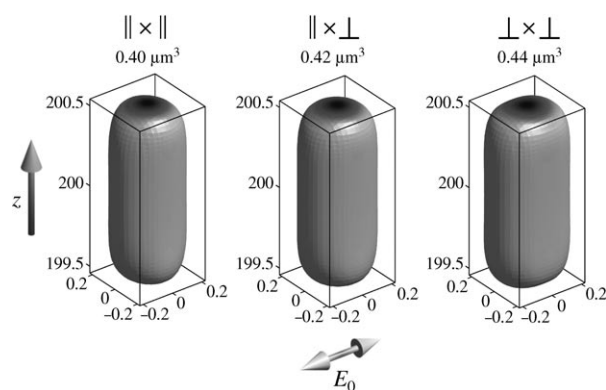


Figure 4. The shape of the MDF for three different detection and correlation schemes, visualized by displaying the isosurfaces where the MDF has fallen to $1/e^2 \approx 13\%$ of its maximum value in the center. The left box shows the MDF of the autocorrelation of the detector signal monitoring fluorescence polarization parallel to the incident laser beam. The right box shows that of the detector signal monitoring fluorescence polarization perpendicular to the incident laser beam. The middle box shows the MDF for the cross-correlation between both detectors. The extreme case of completely anisotropic molecules was studied (where the maximum impact of polarization effects on the ACF is expected). Vertical axis (z) is the optical axis; all values are given in micrometers, $z=0$ is at the surface of the cover slide. The polarization of the incident laser beam (E_0) is also shown. Shading of the isosurfaces indicates distance from the optical axis.

important, only the deviation value enters the calculation. Figure 5 shows the impact of cover-slide thickness on the shape of the MDF and ACF as well as the dependence of the apparently determined diffusion coefficient and concentration on thickness deviation. The latter dependencies were calculated by using the ACF generated by the ideal, aberration-free MDF as a reference.^[33] As can be seen, the additional (respectively missing) layer of glass leads to an elongation of the MDF and a slight shift along the optical axis. The enlargement of

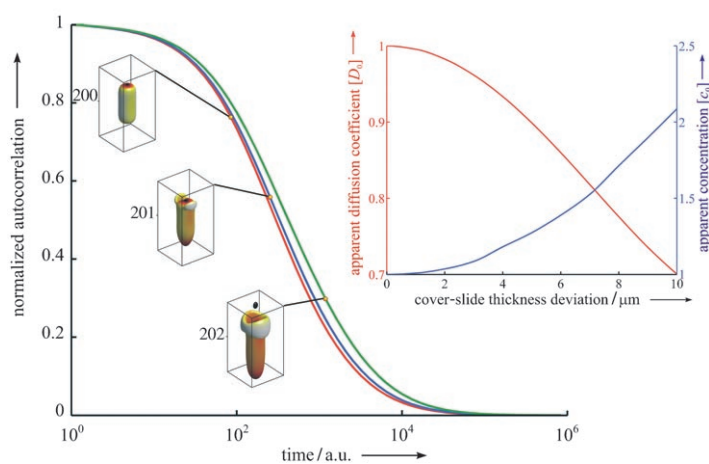


Figure 5. The large figure shows, from left to right, the MDF and ACF for three increasing values of cover-slide thickness deviation, $\delta=0$, $\delta=5$ μm , and $\delta=10$ μm . The box size of the MDF display is $1 \times 1 \times 2 \mu\text{m}^3$; the number next to the box gives the center position along the optical axis in micrometers. Note the shift of the center of the MDF along the optical axis for increasing values of δ . The inset figure shows the dependence of apparent diffusion coefficient and the chemical concentration on thickness deviation value. These values would be obtained when performing a comparative FCS measurement using an ideal ACF ($\delta=0$) as reference (as in the following figures).

the MDF results in increased diffusion times, that is, apparently lower diffusion coefficients, and in an apparently increased concentration (there are more molecules present in the detection volume because the latter has become larger). As will be also seen below, any aberration results in an increased detection volume and thus leads to the same trend of an apparently lower diffusion coefficient and higher concentration with increasing aberration. The impact on the apparent concentration is much stronger than on the apparent diffusion, resulting for example, for a cover-slide thickness deviation of $10\ \mu\text{m}$ to an error of over 100% for the first and of roughly 30% for the second. It should be noted that the calculated errors are not changing significantly when changing the focus position in the solution.

This is in stark contrast to the effect of refractive-index mismatch, which is considered next. An optical microscope using a water-immersion objective is optimally corrected for imaging in water. However, in many biophysical applications, one has to work in buffer solutions with a slightly different refractive index. Also, when measuring in cells or tissues, one faces similarly slight refractive index variations. Typical values of interest are between 1.333 and 1.360. Figure 6 shows the impact of refractive index mismatch on the MDF and ACF and subsequently on the apparent diffusion coefficient and concentration. The impact of even slight refractive-index mismatch is much more dramatic than that of cover-slide thickness. This is mostly due to the large distance of the focus position from the cover-slide surface. In contrast to cover-slide thickness, the aberrations introduced by refractive-index mismatch accumulate with increasing distance of the focus from the cover-slide surface because an increasingly thicker layer of solution with mismatched refractive index lies between the optics and the detection volume. The effect of refractive-index mismatch can be much reduced when positioning the detection volume closer to the surface (e.g. $10\ \mu\text{m}$ away, far enough to avoid fluorescence detection of surface-adsorbed molecules; see also ref. [33]).

The last purely optical effect considered is laser-beam astigmatism, that is, different focal positions within different axial planes. As was already mentioned, astigmatism can be introduced by mirror curvature or by optical waveguides used for guiding the excitation light towards the objective. We assume that the laser-beam incident onto the objective is well collimated and has a circular beam profile at the objective's back entry. This is modeled by setting $w_1 = w_2 = w_0$ and $\zeta_2 = \zeta_1 = \zeta_0$ in Equation (14), leading to a circular beam profile at the position of the objective's back aperture ($z=0$) with beam diameter $w = w_0\sqrt{1 + \zeta_0^2}$ but different focus positions in the x - z and y - z planes. As a measure of astigmatism we use the quantity $\Omega = f^2 \text{NA}^2 \zeta_0 / w^2$,^[45] where f is the focal distance of the objective. We considered Ω -values between 0 and $\pi/4$, corresponding for exam-

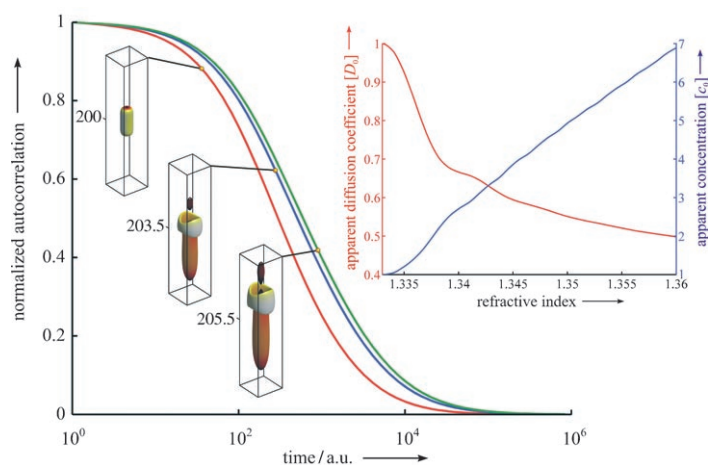


Figure 6. The large figure shows, from left to right, the MDF and ACF for three increasing values of refractive index of the sample solution, $nm = 1.333, 1.346$, and 1.360 . The box size of the MDF displays is $1 \times 1 \times 5\ \mu\text{m}^3$. Note again the shift of the center of the MDF along the optical axis for increasing values of nm . The inset figure shows the dependence of apparent diffusion coefficient and the concentration on refractive index.

ple, to a non-flatness of the dichroic mirror of $\sim \lambda/2$. The resulting shape of the MDF and ACF as well as the apparent diffusion coefficient and chemical concentration are shown in Figure 7. As can be seen, the effect of astigmatism on the measured diffusion and concentration is of a similar magnitude to that of the cover-slide thickness deviation. As for cover-slide thickness, the effect of astigmatism is rather independent of the focal position in the sample. It should be noted that the dramatic change in the shape of the MDF for even slight astigmatism of the exciting laser beam is due to its nearly diffraction-limited focusing. For larger focus diameter and a resulting larger axial extension of the detection volume, the impact of astigmatism will be much less significant.

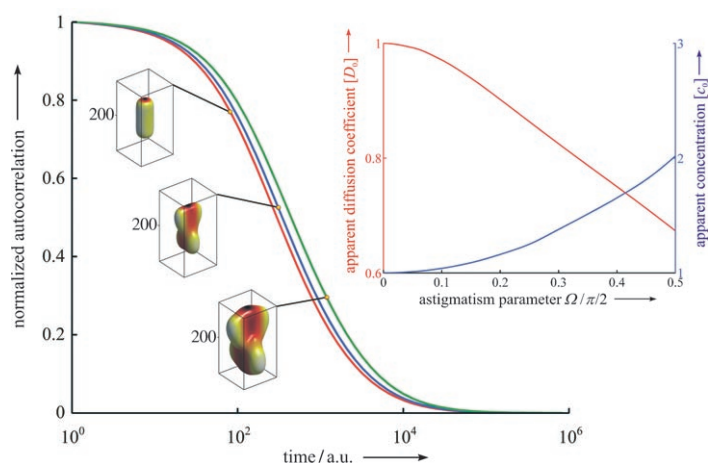


Figure 7. The large figure shows, from left to right, the MDF and ACF for three increasing values of laser beam astigmatism, $\Omega = 0, \Omega = \pi/4$, and $\Omega = \pi/2$. The box size of the MDF-displays is $1 \times 1 \times 2\ \mu\text{m}^3$. There is no shift of the center of the MDF along the optical axis for increasing values of Ω . The inset figure shows the dependence of apparent diffusion coefficient and the concentration on beam astigmatism.

A particularly intriguing effect in an FCS measurement is the dependence of the ACF on the excitation intensity due to optical saturation. The parameter of interest is the optical saturation factor ζ which is defined by $\zeta = \max I_{\text{ex}}/I_{\text{sat}}$ where I_{sat} is the saturation intensity, as defined in Equation (16). This determines how large optical saturation is at the position of strongest fluorescence excitation. Figure 8 shows how optical saturation changes the shape of the MDF and ACF, and how the

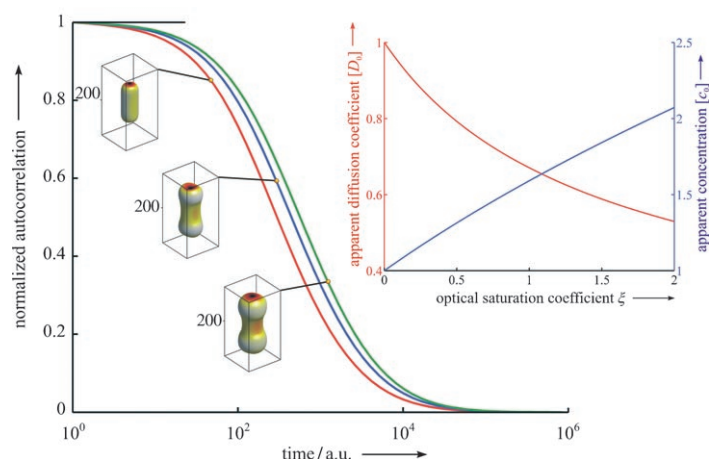


Figure 8. The large figure shows, from left to right, the MDF and ACF for three increasing values of optical saturation, $\zeta = 0$, $\zeta = 1$, and $\zeta = 2$. The box size of the MDF displays is $1 \times 1 \times 2 \mu\text{m}^3$. The inset figure shows the dependence of apparent diffusion coefficient and concentration on optical saturation that is, excitation intensity.

apparent diffusion coefficient and concentration depend on ζ . An important and novel feature is the behavior of the curves of apparent diffusion coefficient and chemical concentration in the limit of vanishing excitation intensity ($\zeta \rightarrow 0$); whereas for all optical effects studied before the slope of these curves tended to zero for vanishing aberration (or astigmatism), its absolute value now is largest at $\zeta = 0$. To understand the reason for that behavior better, consider an ideal Gaussian excitation profile $e^{-x^2/2}$ with mean square deviation of one. Figure 9 shows the widening of such a profile when transformed by a saturation to $e^{-x^2/2}/(1+\zeta e^{-x^2/2})$. As can be seen, a change in the profile width is fastest in the limit $\zeta \rightarrow 0$, explaining why one sees most of the changes in FCS at low saturation levels.

Discussion

We presented results for the impact of cover-slide thickness, refractive index, laser-beam astigmatism, and optical saturation on the MDF, the ACF, and on determining diffusion coefficient and concentration. In practice, one usually measures the ACF for a sample with known diffusion coefficient and concentration and uses that ACF as reference for evaluating the results for the sample of interest. As long as all optical parameters such as cover-slide thickness, refractive index, beam astigmatism, and laser focus position within the sample solution are not changed between reference and sample measurement, and for negligible or equal optical saturation in the reference

and sample, a comparative determination of sample diffusion and concentration with respect to the reference will give correct results. It is straightforward to check whether there is any change in cover-slide thickness, refractive index, and focus position by measuring these values. Also, beam astigmatism will not change from measurement to measurement as long as nothing is changed within the excitation light path.

The situation becomes much more complicated for optical saturation. To estimate realistic values of the saturation parameter ζ , consider a dye having the following photophysical parameters: extinction coefficient of $10^5 \text{ L mol}^{-1} \text{ cm}^{-1}$, fluorescence lifetime of 3 ns, intersystem crossing yield of 0.1 %, and a triplet-state lifetime of 3 μs . Such values are typical for organic dyes such as those used in FCS measurements. The chosen values yield a saturation intensity of $\approx 33.4 \text{ kW cm}^{-2}$.^[36] For the diffraction-limited focus, this corresponds to a total laser power of roughly 125 μW , a typical value used in FCS measurements. The saturation intensity will shift to even smaller values with increasing intersystem crossing yield, triplet-state lifetime, or larger extinction coefficient. Thus, optical saturation should always be taken into account when performing FCS measurements with diffraction limited focusing, that is, high peak excitation intensities. It makes even comparative FCS measurements difficult if the photophysics and thus optical saturation of sample and reference are different. Moreover, many dyes change their photophysical properties, in particular intersystem crossing yield and triplet-state lifetime, upon binding for example, to a protein so that even a comparative measurement between free and bound dye may become flawed. An additional complication is the large slope of the apparent diffusion and concentration curves for vanishing optical saturation. This makes it difficult to extrapolate their correct values for zero optical saturation by determining them at decreasing excitation intensities and extrapolating towards zero intensity. Due to the unknown slope value at zero intensity, the extrapolation will have a large error

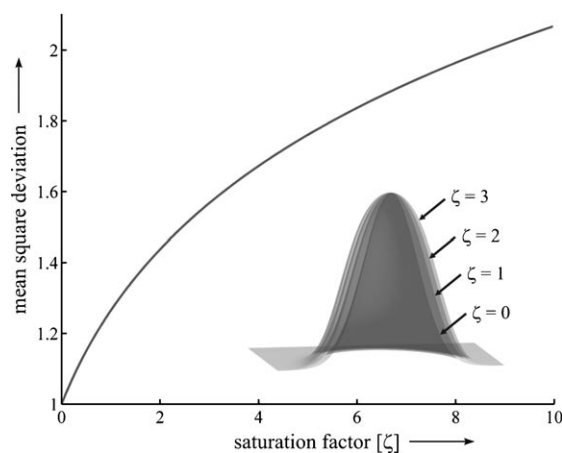


Figure 9. The change of the mean square deviation of the distribution $e^{-x^2/2}/(1+\zeta e^{-x^2/2})$ with increasing value of ζ .

margin. Moreover, when halving the excitation intensity, one needs roughly four times longer to obtain an ACF of similar signal-to-noise quality. This makes the acquisition of reliable data points for decreasing values of ζ increasingly time-consuming.

Many of the discussed problems can be reduced when using larger focus diameters, that is, when not working in the diffraction limit of focusing. This is achieved by coupling into the objective laser beams of smaller diameter. Figure 10 shows the shape of the MDF and the size of the effective detection

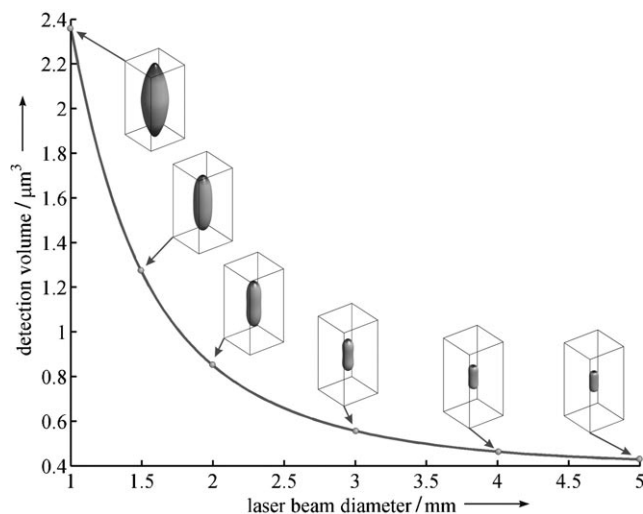


Figure 10. Dependence of detection volume and MDF on incident laser-beam diameter. With increasing beam diameter, the ideal of a diffraction limited focus is approached. Although a smaller laser-beam diameter alleviates many of the aberrational effects discussed in the paper, it makes the absolute size of the detection volume very sensitive with respect to beam diameter. The box size of the MDF displays is $2 \times 2 \times 4 \mu\text{m}^3$.

volume in dependence on the excitation laser-beam diameter. A tighter laser beam results in an effective reduction of the numerical aperture upon focusing. This relaxes many of the aberrational effects discussed above. However, there are several disadvantages of this approach. First, with decreasing laser-beam diameter, the detection volume becomes increasingly sensitive to variations in beam diameter, making measurements less reproducible (see Figure 10). Second, a larger detection volume lowers the concentration range accessible by FCS measurements.^[53] Last but not least, a larger focus diameter demands an increase in the total excitation power to achieve comparable maximum count rates per molecule. This usually leads to the introduction of photobleaching effects, which were completely neglected in our considerations. Photobleaching destroys the *stationarity* of an FCS measurement, that is, the invariance of the ACF with respect to absolute time shifts, which makes its theoretical treatment enormously complicated and far beyond the scope of the present paper; but see refs. [54–56]. Photobleaching is usually not an issue when using diffraction-limited focusing, resulting in very short residence times of molecules within the detection volume (a few dozen microseconds).

An important question is whether it is possible to recognize any of the discussed artifacts by analyzing the shape of the

measured ACF. For that, it would be necessary that the ACF in the presence of artifacts can be distinguished from a perfect ACF. For an ideal measurement system, changing the diffusion coefficient of the sample leads to a rescaling of the temporal axis, which appears as a parallel shift of the ACF along the time axis in a time-logarithmic plot. The ACFs in Figures 5 and 6 indicate that the aberrations introduced by cover-slide thickness deviation and refractive-index mismatch lead to shapes of the ACF which cannot be obtained by rescaling the temporal axis. Thus, the presence of such aberrations can indeed be discovered by comparing a measurement with an aberration-free reference measurement. The situation is different for beam astigmatism and optical saturation, as seen in Figures 7 and 8. The ACFs changed by astigmatism or saturation are very similar to ideal ACFs for samples with slower diffusion coefficients. Thus, it is generally impossible to distinguish between such cases by simply checking the shape of the ACF.

A criterion proposed by Hess and Webb^[32] for recognizing deviations of the MDF from a supposedly ideal 3D Gaussian distribution was to measure counts per molecule (CPM) at changing values of the confocal aperture diameter. Knowing the average fluorescence intensity and the average number of molecules in the detection volume, the CPM is calculated as the ratio of both numbers and is proportional, for a background-free measurement, to $\int dr U^2(\mathbf{r}) / \int dr U(\mathbf{r})$.^[32] They demonstrated that, for an ideal three-dimensional Gaussian MDF, the CPM is basically independent of aperture diameter, whereas for more realistic MDFs this value, after reaching some maximum at low aperture diameter, steadily decreases for increasing aperture diameter. Krouglova et al.^[57] used that criterion in their FCS measurements with a Confocor 2 to check for significant deviations of the MDF from the ideal 3D Gaussian. Surprisingly, they did not discover any maximum in the CPM as predicted by Hess and Webb, but found a curve which rather resembled that expected for a perfect 3D Gaussian. What probably happened was a slight misalignment of the aperture position along the optical axis. This is demonstrated by Figure 11; it shows the calculated CPM for varying aperture diameter and for different values of aperture misalignment along the optical axis. As can be seen, the qualitative dependence of the CPM on aperture diameter can be completely inverted when shifting the aperture along the optical axis. Surprisingly, when trying to fit the resulting ACFs with the standard model based on a 3D Gaussian MDF, the fit quality becomes even better for increasing misalignment, being nearly perfect for a misalignment value of 2 mm. This is also in accordance with the experimental results reported in ref. [57], where the authors took the nearly perfect fit of their measured ACFs by the standard model as an additional proof of the perfect 3D Gaussian shape of their MDF, which is by far not the case for a 2-mm misalignment of the aperture (see Figure 11). Thus, the criterion of perfect “fitability” of an ACF by the standard model based on a 3D Gaussian MDF is also not a reliable check for the factual presence of such a MDF or the absence of any artifacts. Fortunately, for the final conclusions of ref. [57], that was of no importance because the authors made comparative measurements of diffusion coefficients using rhodamine 6G as the ref-

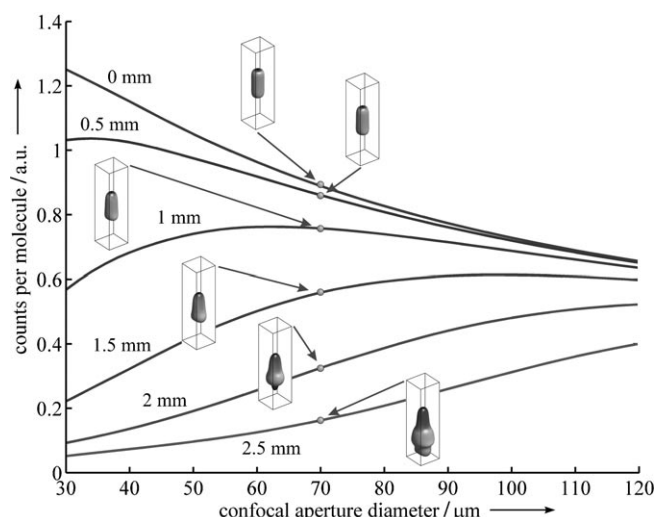


Figure 11. Dependence of counts per molecule and MDF on the confocal aperture diameter for different aperture positions along the optical axis (out of the image plane). For increasing displacement of the aperture, the qualitative dependence of counts per molecule on aperture diameter is completely reversed. The box size of the MDF displays is $0.8 \times 0.8 \times 3 \mu\text{m}^3$.

erence. Moreover, the probable misalignment of the aperture had the additional effect that detection efficiency was maximum before (or after) the excitation intensity reached its maximum along the optical axis, thus alleviating also potential optical saturation effects (at the cost of a longer measurement time).

Conclusions

We have developed an exhaustive theoretical framework for the exact modeling of FCS measurements, in particular the diffusion-related part of an ACF. The experimentally most important artifacts of FCS were considered in detail. As was demonstrated, an ACF is very sensitive to even slight optical aberration or saturation. In case of beam astigmatism or saturation, it is moreover rather impossible to distinguish between an ACF in the presence of these effects and an ACF measured on a sample with slower diffusion coefficient. Also, the CPM criterion or the criterion of fit quality with the standard model fit based on a 3D Gaussian MDF can be misleading. The best advice that can be given is to try to control as many as possible of the discussed optical parameters (cover-slide thickness, sample refractive index, beam astigmatism), and to measure at rather moderate excitation intensities. Taking a series of measurements with varying excitation intensity will always be a good choice for checking the dependence of the apparent diffusion coefficient and concentration on intensity.

Acknowledgments

We thank Thomas Ruckstuhl for his many valuable comments and corrections. We are grateful to the Deutsche Forschungsgemeinschaft and the Deutsche Volkswagenstiftung for their financial support.

Keywords: confocal microscopy · fluorescence spectroscopy · laser spectroscopy · photophysics · single-molecule spectroscopy

- [1] D. Magde, E. Elson, W. W. Webb, *Phys. Rev. Lett.* **1972**, *29*, 705–708.
- [2] E. L. Elson, D. Magde, *Biopolymers* **1974**, *13*, 1–27.
- [3] D. Magde, E. Elson, W. W. Webb, *Biopolymers* **1974**, *13*, 29–61.
- [4] R. Rigler, J. Widengren, *Bioscience* **1990**, *3*, 180–183.
- [5] J. Korlach, P. Schwille, W. W. Webb, G. W. Feigenson, *Proc. Natl. Acad. Sci. USA* **1999**, *96*, 8461–8466.
- [6] C. Gell, D. J. Brockwell, G. S. Beddard, S. E. Radford, A. P. Kalverda, D. A. Smith, *Single Mol.* **2001**, *2*, 177–181.
- [7] N. Yoshida, M. Tamura, M. Kinjo, *Single Mol.* **2001**, *2*, 279–283.
- [8] J. Widengren, R. Rigler, *Cell. Mol. Biol. Res.* **1998**, *44*, 857–879.
- [9] S. Björling, M. Kinjo, Z. Földes-Papp, E. Hagman, P. Thyberg, R. Rigler, *Biochemistry* **1998**, *37*, 12971–12978.
- [10] K. Häsler, O. Pänke, W. Junge, *Biochemistry* **1999**, *38*, 13759–13765.
- [11] P. Schwille, J. Bieschke, F. Oehlenschläger, *Biophys. Chem.* **1997**, *66*, 211–228.
- [12] T. Wohland, K. Friedrich, R. Hovius, H. Vogel, *Biochemistry* **1999**, *38*, 8671–8681.
- [13] K. G. Heinze, M. Rarbach, M. Jahnz, P. Schwille, *Biophys. J.* **2002**, *83*, 1671–1681.
- [14] U. Kettling, A. Koltermann, P. Schwille, M. Eigen, *Proc. Natl. Acad. Sci. USA* **1998**, *95*, 1416–1420.
- [15] J. Widengren, Ü. Mets, R. Rigler, *Chem. Phys.* **1999**, *250*, 171–186.
- [16] U. Haupts, S. Maiti, P. Schwille, W. W. Webb, *Proc. Natl. Acad. Sci. USA* **1998**, *95*, 13573–13578.
- [17] A. A. Heikal, S. T. Hess, G. S. Baird, R. Y. Tsien, W. W. Webb, *Proc. Natl. Acad. Sci. USA* **2000**, *97*, 11996–12001.
- [18] R. Brock, G. Vámosi, G. Vereb, T. M. Jovin, *Proc. Natl. Acad. Sci. USA* **1999**, *96*, 10123–10128.
- [19] A. A. Heikal, S. T. Hess, W. W. Webb, *Chem. Phys.* **2001**, *274*, 37–55.
- [20] P. Schwille, S. Kummer, A. A. Heikal, W. E. Moerner, W. W. Webb, *Proc. Natl. Acad. Sci. USA* **2000**, *97*, 151–156.
- [21] J. Widengren, C. A. M. Seidel, *Phys. Chem. Chem. Phys.* **2000**, *2*, 3435–3441.
- [22] S. Huang, A. A. Heikal, W. W. Webb, *Biophys. J.* **2002**, *82*, 2811–2825.
- [23] F. Malvezzi-Campeggi, M. Jahnz, K. G. Heinze, P. Dittrich, P. Schwille, *Biophys. J.* **2001**, *81*, 1776–1785.
- [24] J. Widengren, P. Schwille, *J. Phys. Chem. A* **2000**, *104*, 6416–6428.
- [25] J. Widengren, Ü. Mets in *Single-Molecule Detection in Solution—Methods and Applications* (Eds.: C. Zander, J. Enderlein, R. A. Keller), Wiley-VCH, Berlin, **2002**, pp. 69–95.
- [26] *Fluorescence Correlation Spectroscopy* (Eds.: R. Rigler, E. Elson), Springer, Berlin, **2001**.
- [27] P. Schwille, *Cell Biochem. Biophys.* **2001**, *34*, 383–408.
- [28] S. T. Hess, S. Huang, A. A. Heikal, W. W. Webb, *Biochemistry* **2002**, *41*, 697–705.
- [29] P. Kask, P. Piksarv, Ü. Mets, *Eur. Biophys. J.* **1985**, *12*, 163–166.
- [30] P. Kask, P. Piksarv, Ü. Mets, M. Pooga, E. Lippmaa, *Eur. Biophys. J.* **1987**, *14*, 257–261.
- [31] R. Rigler, Ü. Mets, J. Widengren, P. Kask, *Eur. Biophys. J.* **1993**, *22*, 169–175.
- [32] S. T. Hess, W. W. Webb, *Biophys. J.* **2002**, *83*, 2300–2317.
- [33] J. Enderlein, I. Gregor, D. Patra, J. Fitter, *Curr. Opin. Pharmacol. Biotechnol.* **2004**, *5*, 155–161.
- [34] K. Berland, G. Shen, *Appl. Opt.* **2003**, *42*, 5566–5576.
- [35] G. Nishimura, M. Kinjo, *Anal. Chem.* **2004**, *76*, 1963–1970.
- [36] I. Gregor, D. Patra, J. Enderlein, *ChemPhysChem* **2005**, *6*, 164–170.
- [37] M. Böhmer, J. Enderlein in *Single-Molecule Detection in Solution—Methods and Applications* (Eds.: C. Zander, J. Enderlein, R. A. Keller), Wiley-VCH, Berlin, **2002**, pp. 145–183.
- [38] J. Widengren, Ü. Mets, R. Rigler, *J. Phys. Chem.* **1995**, *99*, 13368–13379.
- [39] J. B. Pawley, *Handbook of Biological Confocal Microscopy*, Kluwer, Dordrecht, **1995**.
- [40] *Optical Imaging and Microscopy: Techniques and Advanced Systems* (Eds.: P. Török, F.-J. Kao), Springer, **2004**.

- [41] D. Patra, I. Gregor, J. Enderlein, M. Sauer, *Appl. Phys. Lett.* **2005**, *87*, 101103.
- [42] E. Wolf, *Proc. R. Soc. London Ser. A* **1959**, *253*, 349–357.
- [43] B. Richards, E. Wolf, *Proc. R. Soc. London Ser. A* **1959**, *253*, 358–379.
- [44] M. Born, E. Wolf, *Principles of Optics*, Pergamon, New York, **1985**, ch. 4.6, pp. 169–171.
- [45] I. Gregor, J. Enderlein, *Opt. Lett.* **2005**, *30*, 2527–2529.
- [46] J. Enderlein, *Chem. Phys. Lett.* **2005**, *410*, 452–456.
- [47] J. R. Lakowicz, *Principles of Fluorescence Spectroscopy*, Kluwer, New York, **1999**, ch. 12.2, p. 349.
- [48] S. R. Aragón, R. Pecora, *Biopolymers* **1975**, *14*, 119–138.
- [49] C. J. R. Sheppard, P. Török, *Bioimaging* **1997**, *5*, 205–218.
- [50] P. Török, P. D. Higdon, T. Wilson, *J. Mod. Opt.* **1998**, *45*, 1681–1698.
- [51] P. Török, *Opt. Lett.* **2000**, *25*, 1463–1465.
- [52] J. Enderlein, M. Böhmer, *Opt. Lett.* **2003**, *28*, 941–943.
- [53] J. Enderlein, I. Gregor, D. Patra, J. Fitter, *J. Fluoresc.* **2005**, *15*, 415–422.
- [54] J. Widengren, R. Rigler, *Bioimaging* **1996**, *4*, 149–157.
- [55] C. Eggeling, J. Widengren, R. Rigler, C. A. M. Seidel, *Anal. Chem.* **1998**, *70*, 2651–2659.
- [56] P. S. Dittrich, P. Schwille, *Appl. Phys. B* **2001**, *73*, 829–837.
- [57] T. Krouglova, J. Vercaemmen, Y. Engelborghs, *Biophys. J.* **2004**, *87*, 2635–2646.

Received: July 27, 2005